JOURNAL OF COMPUTATIONAL PHYSICS **138,** 644–664 (1997)
ARTICLE NO. CP975837

Wind Set-down Relaxation on a Sloping Beach

Anne Gelb,* David Gottlieb,† and Nathan Paldor‡

CRPC Mail Code 217-50, California Institute of Technology, Pasadena, CA 91125; †Division of Applied Mathematics, Brown University, Providence, Rhode Island 02912; and ‡Department of Atmospheric Sciences, The Hebrew University of Jerusalem, Jerusalem, 91904, Israel

Received March 18, 1997

Consider a long and narrow basin where both the Coriolis force and the dynamics in the cross-basin direction can be neglected. The bottom of the basin is assumed to slope linearly from the head of the basin toward its mouth, where the water is infinitely deep. The shape of the sea surface in the steady-state solution of the ''wind set-down'' problem is determined by the balance between the wind which blows over the basin from the shore seaward and the pressure gradient which results from the slope of the sea surface. This study addresses the time-dependent problem encountered when the wind in the wind set-down solution suddenly relaxes and the water gushes landward under the influence of the pressure gradient force. We call this problem the ''relaxation of the wind set-down.'' The difficulty in solving this problem is due to the moving singularity associated with the ever-changing location of the point where the sea surface intersects the sloping bottom. At this point the problem is only *weakly hyperbolic*, thus only *weakly well posed*. We solve this problem numerically using two completely different types of numerical solvers, finite difference schemes and spectral methods. Both types of solvers are successfully tested on a similar problem where the analytical solution is known. Both the MacCormack finite difference scheme and the Chebyshev spectral method concurred in their results, strongly suggesting the validity of the numerical solution. Our results indicate that no wave breaking occurs and that the water will slosh up and down the sloping bottom, similar to the behavior of a nonlinear gravity wave. The spectrum of this wave motion consists of peaks associated with the motion of regular gravity waves in a triangular basin, as well as frequency beatings associated with the movement of the singular point of the present problem.

Key Words: shallow water equations; sloping beach; weakly hyperbolic; moving singularity; spectral methods.

0021-9991/97 $25.00

1. INTRODUCTION

1.1. *General Background*

Consider a long and narrow basin, such as the Gulf of Suez, the Gulf of Elat, or Baja California, neglecting both the Coriolis force and the dynamics in the cross-basin direction. The bottom of the gulf slopes linearly toward the mouth of the gulf, where the deep water begins (see Fig. 1). The steady-state solution for the flow in which the wind blows over the water from the short seaward, where the vertically averaged water velocity is identically zero, results from the balance between the wind stress acting at the top of the water column and the vertically integrated pressure gradient resulting from the slope of the sea surface [10]. The uniform wind stress equally distributed throughout the entire water column is directed seaward, and thus the slope of the sea surface, providing the balancing pressure gradient, is directed landward. The thickness of the water column decreases landward as a result of the bottom slope, causing the sea surface slope to increase drastically at the point where the water depth vanishes at the shoreline. The resulting shape of the sea surface in Fig. 1 is an implicit function of the distance from land determined by the wind stress and the geometry of the gulf. Once this steady-state solution is reached, it will continue to hold for as long as the wind speed and direction blowing over the gulf remain unchanged. This problem is known as the wind set-down problem, as it deals with the case when the wind lowers the sea surface relative to its level state. It is the analog of the wind set-up problem encountered when the wind pushes the water against the coast causing the sea level to ascend *above* its level.

In this study we address the problem encountered when the water is initially in the wind set-down steady-state solution, and the wind blowing over the water suddenly calms down. At the moment directly preceding the cessation of the wind,

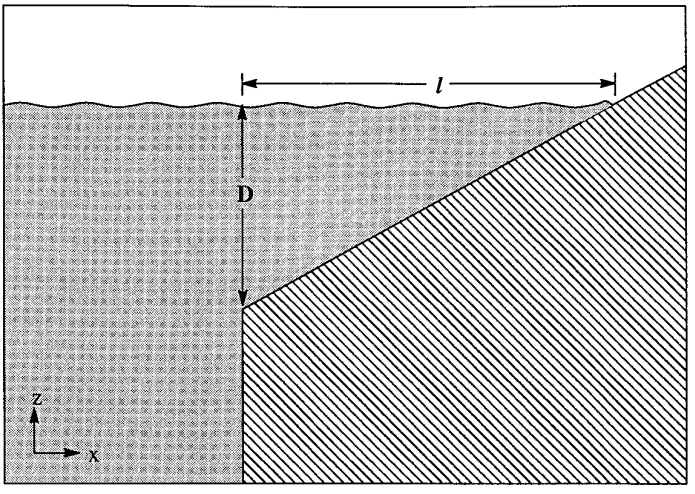

FIG. 1. Schematic diagram of the gulf, which is taken to be a long and narrow channel with a linearly sloping bottom.

the sloping sea surface still provides a pressure gradient that accelerates the still water toward the land. This acceleration is proportional to the sea surface slope, and since this slope increases toward the land, the water closest to land will tend to have greater velocity than the water further seaward. Thus the sea surface is expected to ''flatten,'' at least for a short time, following the cessation of the wind. We call this problem the ''relaxation of the wind set-down,'' as it deals with the return of the sea surface and water velocity from the steady-state solution of the wind set-down problem back to the calm and level sea surface solution.

1.2. *Time-Dependent Flow on a Linearly Sloping Beach*

The inviscid and time-dependent flow of water on a sloping beach has been long recognized as an important problem both theoretically and practically. Theoretically, the problem is challenging due to the moving singularity associated with the ever-changing location of the point (or a line in the two-dimensional model) where the sea surface intersects the sloping bottom. At this point of total vanishing water depth, the equations cease to be strongly hyperbolic. From a practical standpoint, a good grasp of this problem is crucial for planning for such catastrophic events as storm surges climbing up a beach, erosion of beach fronts, and the landward march of long gravity waves, such as tsunamis, pounding on the coast as a result of an earthquake somewhere in the open ocean off the coast.

Stoker [11] was the first to address this problem by formulating the governing nonlinear partial differential equations for the one-dimensional case of a simple linearly sloping bottom. He analytically solved for the characteristic curves of the equations and detailed occurring shock formations. Later in [4] problems for which the analytical solutions were not feasible were numerically calculated, and the evolution of the sea surface and water velocity were accurately predicted for a similar dam-breaking problem. Further advances in the problem were obtained when it was realized [3, 7] that in the special case of a linearly sloping bottom, the nonlinear equations can be transformed into linear equations. The solutions of these similarity transformations describe a periodic motion of the water up and down the beach with no wave breaking and no dissipation of the wave motion over time. For other types of initial perturbations, such as compressive waves, the nonlinear waves which develop can break and form shocks. Thus shock formation depends on the initial conditions, and there are no general criteria which can predict whether or not shocks will be formed.

Some further progress in this direction was achieved in the same linearly sloping bottom case where it was shown that the resulting integral equation can be solved for arbitrary initial conditions by applying a Laplace or Hankel transformation to the linearized version of the governing partial differential equations [12]. This, along with a transformation similar to that in [3], made it possible to solve the initial value problem for a certain class of initial conditions.

By applying finite difference schemes to the initial value problem associated with an advancing bore, or more specifically a vertical ''wall'' of turbulent water moving ahead of a rather smooth and elevated sea surface, a direct numerical solution in the context of tsunami modeling was simulated in [8]. The immediate vicinity of

the singular point where the water depth vanishes is discarded and the governing equation is integrated only up to a short distance behind this point. This solution ignores the dynamics associated with the ''tip'' of the advancing bore and concludes that these bores will slosh up and down the beach with no appreciable change in this amplitude. The wave's amplification amplitude approaching the beach, the incoming tsunami distance, and the wave-breaking criterion were calculated in [9].

In this paper we solve the problem of ''relaxation of the wind set-down'' numerically and conclude that no wave breaking occurs. We also determine the frequency of the waves.

1.3. *Numerical Background*

As mentioned above, the difficulty of this problem is due to the moving singularity associated with the ever changing location of the point where the sea surface intersects the sloping bottom. Furthermore, in the mathematical analysis one discovers that the eigenvalues at this point are both real and equivalent, implying that the associated Jacobian matrix is not diagonalizable. From elementary theory of numerical analysis for hyperbolic equations, we know that this indicates that the problem is only *weakly hyperbolic* at this point and therefore only weakly well posed.

We approached this problem using both finite difference schemes and spectral methods. Finite difference methods are local methods that involve finding a solution for a particular grid point in time and space based on the information provided by its neighboring grid points. They are known to work very well for strongly well-posed problems, but the results are inconclusive for weakly well-posed problems. We employed two different finite difference schemes. The Lax Friedrich's method is first order in time and space and also handles shock discontinuities, but it suffers from dissipation for long time solutions. The MacCormack method is second order and has less dissipation, but will not perform well if there are shocks in the solution. Since it became apparent that no shocks would be formed, we dropped the Lax Friedrich's scheme from our study and concentrated on the MacCormack method instead.

Spectral methods are global methods obtained by expanding a function in terms of orthogonal basis functions [6]. For the Chebyshev collocation method, $f(x, t)$ defined in the interval $[-1, 1]$ is approximated by

$$f_N(x, t) = \sum_{k=0}^{N} a_k(t) T_k(x),$$

where the basis functions $T_k(x)$ are defined by

$$T_k(x) = \cos(k \cos^{-1} x)$$

and the coefficients $a_k(t)$ are

$$a_k(t) = \frac{2}{N c_k} \sum_{j=0}^{N} \frac{f(x_j, t) T_k(x_j)}{c_j},$$

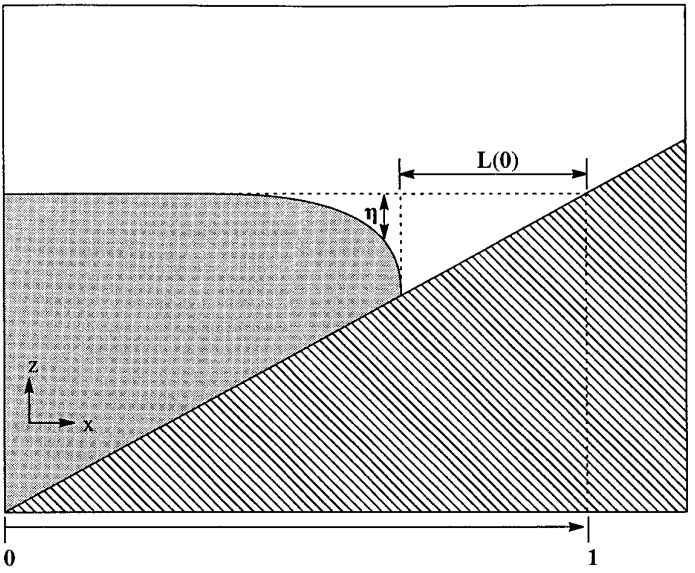

FIG. 2. Initial condition $\eta(x, 0)$. Note that $\partial\eta(1 - L(0), 0)/\partial x \to -\infty$.

where $c_i = 1$ for $i = 1, \ldots, N - 1$ and $c_i = 2$ for $i = 0, N$. The collocation points x_j are given by

$$x_j = \cos\frac{\pi j}{N}, \qquad j = 0, \ldots, N.$$

The Chebyshev points are placed more densely at the boundaries than in the interior of the domain, implying that the Chebyshev method is particularly well suited for problems where the solution varies drastically near the boundaries. The Chebyshev spectral method will not work if discontinuities are present in the solution.

Our solution to the wind-set down relaxation problem is valid since both the MacCormack and Chebyshev methods concur in their results. In fact these methods are valid for any basin, and we use the example above because of its important consequences.

2. THE RELAXATION OF THE WIND SET-DOWN MODEL

2.1. *The Nonlinear Hyperbolic System*

Consider the nondimensional hyperbolic system which describes the shallow water dynamics of the linearly sloping gulf shown in Fig. 1, where u is the vertically averaged velocity of the water and η is the sea surface height above still level

$$\begin{aligned} u_t &= -\left(\eta + \frac{1}{2}u^2\right)_x \\ \eta_t &= -(u(1 - x + \eta))_x \end{aligned} \tag{2.1}$$

inside the domain

$$0 \leq x \leq 1 - L(t),$$

where $L(t) < 1$, the time-dependent distance from the shoreline to the point where the total depth of the water vanishes, is defined by

$$L(t) = -\eta(1 - L(t), t). \tag{2.2}$$

Denoting $\hat{x}$, $\hat{u}$, $\hat{\eta}$, and $\hat{t}$ as the dimensional quantities, the nondimensional quantities are obtained (as shown in [3]), by defining $x = \hat{x}/l$, $\eta = \hat{\eta}/D$, $u = \hat{u}/\sqrt{gD}$, and $t = \hat{t}\sqrt{gD}/l$, where l is the length of the gulf when the sea surface is level, D is the total depth of the water, and g is the acceleration due to gravity (Fig. 1). The sea surface height, $\eta(x, t)$, is negative for receding water, whereas $L(t)$ is positive in this case.

The water is initially at rest

$$u(x, 0) = 0 \tag{2.3}$$

and the initial sea surface height is given implicitly by the steady-state solution of the wind set-down solution described in [10]

$$x = \eta(x, 0) + (1 - \gamma)(1 - e^{\frac{-\eta(x,0)}{\gamma}}), \tag{2.4}$$

where the parameter γ, determined by the geometry of the gulf and the wind stress, has typical value of

$$-0.02 \leq \gamma \leq -0.01,$$

implying that $\eta(x, 0) \leq 0$. For $D \approx 70$ m and $l \approx 350$ km, the wind stress is approximately $10^{-4}\text{m}^2/\text{s}^2$.

For this choice of $\eta(x, 0)$, the distance from the shoreline to the point where the total depth of the water vanishes is initially

$$L(0) = -\gamma ln(1 - 1/\gamma).$$

The system (2.1), along with the initial conditions (2.3) and (2.4), describes the dynamics of the water in the gulf when the wind calms down so that the pressure gradient force, which was balaned by the wind stress, accelerates the water landward. The left boundary condition for η is

$$\eta(0, t) = 0. \tag{2.5}$$

This allows gravity waves to radiate in and out of the gulf through its mouth by tilting the sea surface there, while still allowing the surface at $x \leq 0$ to remain constant at the (infinitely deep) ocean even when water enter and leaves the mouth of the gulf.

Two separate cases are considered for the right boundary (shoreline). In the first case we consider a moving domain, where the only requirement is regularity of the solution at $x = 1 - L(t)$. Thus no boundary condition is given for $u(1 - L(t), t)$ and the velocity is determined dynamically.

In the second simpler case, primarily studied to verify the results of the first case, the domain is fixed by placing a wall at some point $x = x_0$ (e.g., $x_0 = 0.95$). In this case, the right boundary condition

$$u(x_0, t) = 0$$

is imposed, and $L(t)$ now measures the depression of the water at the wall

$$L(t) = -\eta(x_0, t). \tag{2.6}$$

The Jacobian of system (2.1) is

$$\begin{pmatrix} u & 1 \\ 1 - x + \eta & u \end{pmatrix}$$

with eigenvalues

$$\lambda_1 = u + \sqrt{1 - x + \eta}$$
$$\lambda_2 = u - \sqrt{1 - x + \eta}$$

and corresponding Riemann invariants

$$s_1 = u + 2\sqrt{1 - x + \eta} + t$$
$$s_2 - u + 2\sqrt{1 - x + \eta} + t.$$

System (2.1) is strictly hyperbolic for $1 - x + \eta \geq 0$, but if $1 - x + \eta < 0$, the problem loses hyperbolicity and is no longer well posed. Furthermore, at $x = 1 - L(t)$ the eigenvalues $\lambda_1 = \lambda_2 = u$. Therefore the problem at the right boundary is only weakly hyperbolic, and hence, even in the linear case, only weakly well posed. This delicate boundary is the crux of the numerical problem.

System (2.1) also has an entropy function $\Phi(u, \eta)$ and a corresponding entropy flux $\Psi(u, \eta)$

$$\Phi(u, \eta) = \frac{\eta^2}{2} + (1 - x + \eta)\frac{u^2}{2}$$

$$\Psi(u, \eta) = u\left(\eta + \frac{\eta^2}{2}\right)(1 - x + \eta),$$

such that

$$\Phi(u, \eta)_t + \Psi(u, \eta)_x = 0.$$

2.2. *Transformation of System (2.1)*

In this section system (2.1) is transformed in order to make it amenable for the numerical solution. We "freeze" the boundary of system (2.1) such that the moving domain $x \in [0, 1 - L(t)]$ translates to the stationary domain $\xi \in [0, 1]$. This transformation applies only to the case where $L(t)$ is defined by (2.2), since the "wall" problem is already defined in a fixed domain.

Defining

$$\begin{aligned} \xi &= \frac{x}{1 - L(t)} \\ t &= t \\ \omega_1(\xi, t) &= (1 - x + \eta(x, t))(1 - L(t)) \\ \omega_2(\xi, t) &= (1 - x + \eta(x, t))(u(x, t) + t)((1 - L(t)), \end{aligned} \tag{2.7}$$

and substituting the transformation equations (2.7) into the system (2.1), yields

$$\begin{aligned} \frac{\partial \omega_1}{\partial t} + \frac{1}{(1 - L(t))}((L'\xi - t)\omega_1 + \omega_2)_\xi &= 0 \\ \frac{\partial \omega_2}{\partial t} + \frac{1}{(1 - L(t))}\left((L'\xi - t)\omega_2 + \frac{\omega_2^2}{\omega_1} + \frac{\omega_1^2}{2(1 - L(t)_\xi}\right)_\xi &= 0, \end{aligned} \tag{2.8}$$

where $L' = L'(t) = dL/dt$.

The initial conditions become

$$\begin{aligned} \omega_2(\xi, 0) &= 0 \\ 0 &= \frac{\omega_1}{1 - L(0)} - 1 + (1 - \gamma)(1 - e^{-(\frac{\omega_1}{1 - L(0)} + (1 - L(0))\xi - 1)/\gamma}). \end{aligned}$$

The parameter t has not changed. The boundary conditions are

$$\begin{aligned} \omega_1(0, t) &= 1 - L(t) \\ \omega_1(1, t) &= 0 \\ \omega_2(1, t) &= 0. \end{aligned} \tag{2.9}$$

L' is obtained by first noting that the boundary condition implies that $(\partial\omega_1/\partial t)(1, t) = 0$ and then solving

$$\frac{1}{(1 - L(t))}((L'\xi - t)\omega_1 + \omega_2)_\xi = 0.$$

If we define

$$\begin{aligned} D\omega_1 &= \frac{\partial \omega_1}{\partial \xi}(1,t) \\ D\omega_2 &= \frac{\partial \omega_2}{\partial \xi}(1,t), \end{aligned} \tag{2.10}$$

then L' satisfies the equation

$$L' = t - \frac{D\omega_2}{D\omega_1}. \tag{2.11}$$

The same equation for L' is obtained by solving $(\partial\omega_2/\partial t)\,(1,\,t) = 0$.

System (2.8) has an advantage over the original system (2.1) in that boundary conditions are imposed on both variables ω_1 and ω_2. This additional boundary condition is a result of the implicit requirement that $u(x, t)$ is finite at $x = 1 - L(t)$. On the other hand, a new variable to the problem, $L'(t)$, has been added. Although $L'(t)$ is solved only at $\xi = 1$, it is inherent in the flux throughout the entire domain. Solving $L'(t)$ becomes the critical element of the problem.

The Jacobian of system (2.8) is

$$\begin{bmatrix} \dfrac{\xi L' - t}{1 - L(t)} & \dfrac{1}{1 - L(t)} \\ \dfrac{\omega_2^2/\omega_1^2 + \omega_1/(1 - L(t))}{1 - L(t)} & \dfrac{\xi L' - t + 2\omega_2/\omega_1}{1 - L(t)} \end{bmatrix},$$

with eigenvalues

$$\begin{aligned} \lambda_1 &= \frac{\xi L' - t + \dfrac{\omega_2}{\omega_1} + \sqrt{\dfrac{\omega_1}{1 - L(t)}}}{1 - L(t)} \\ \lambda_2 &= \frac{\xi L' - t + \dfrac{\omega_2}{\omega_1} - \sqrt{\dfrac{\omega_1}{1 - L(t)}}}{1 - L(t)}, \end{aligned} \tag{2.12}$$

implying again that system (2.8) will not be well posed for $\omega_1 < 0$, and also that at $\xi = 1$ the system is only weakly well posed, since $\lambda_1 = \lambda_2 = 0$. The corresponding Riemann invariants are

$$\begin{aligned} s_1 &= \frac{\omega_2}{\omega_1} + 2\sqrt{\frac{\omega_1}{1 - L(t)}} \\ s_2 &= \frac{\omega_2}{\omega_1} - 2\sqrt{\frac{\omega_1}{1 - L(t)}}. \end{aligned} \tag{2.13}$$

3. NUMERICAL METHODS

Both finite difference and spectral schemes were implemented for system (2.8) and then the results were transformed back to the original variables u and η.

The standard MacCormack scheme was applied to the interior points of system (2.8). At the boundaries $\omega_1(1, t) = \omega_2(1, t) = 0$, and $\omega_1(0, t) = 1 - L(t)$ were analytically imposed, while $\omega_2(0, t)$ was numerically solved by a second-order extrapolation of the outflow Riemann invariant corresponding to the negative eigenvalue at $\xi = 0$. More specifically, the eigenvalues in Eq. (2.12) of system (2.8) satisfy $\lambda_1 > 0$ and $\lambda_2 < 0$ for $\xi \in [0, 1)$. Therefore s_2 in Eq. (2.13) is the outflow Riemann invariant at $\xi = 0$. Thus

$$\omega_2(0, t) = \omega_1(0, t)\left[2s_2(\Delta\xi, t) - s_2(2\,\Delta\xi, t) + 2\sqrt{\frac{\omega_1(0, t)}{1 - L(t)}}\right],$$

where

$$s_2(\Delta\xi, t) = \frac{\omega_2(\Delta\xi, t)}{\omega_1(\Delta\xi, t)} - 2\sqrt{\frac{\omega_1(\Delta\xi, t)}{1 - L(t)}}$$

$$s_2(2\Delta\xi, t) = \frac{\omega_2(2\Delta\xi, t)}{\omega_1(2\Delta\xi, t)} - 2\sqrt{\frac{\omega_1(2\Delta\xi, t)}{1 - L(t)}}.$$

L' was numerically solved with accuracy of $O(\Delta\xi)^2$ by

$$L'(t) = t - \frac{D\omega_2(N\Delta\xi, t)}{D\omega_1(N\Delta\xi, t)},$$

where

$$D\omega_i(N\Delta\xi, t) = \frac{3\omega_i(N\Delta\xi, t)}{2\Delta\xi} - \frac{2\omega_i((N-1)\Delta\xi, t)}{\Delta\xi} + \frac{\omega_i((N-2)\Delta\xi, t)}{2\Delta\xi},$$

for $i = 1, 2$ and $\omega_i(N\Delta\xi, t) = \omega_i(1, t) = 0$. Finally, a second-order approximation to $L(t + \Delta t)$ was obtained by

$$L(t + \Delta t) = L(t) + \frac{\Delta t}{2}(L'(t + \Delta t) + L'(t)).$$

The spectral Chebyshev collocation method in space was implemented together with a fourth-order Runge–Kutta scheme in time. The right boundary conditions $\omega_1(1, t) = \omega_2(1, t) = 0$ were imposed at each intermediate stage in the Runge–Kutta time stepping and at the left boundary $\omega_1(0, t)$ was analytically imposed while the Riemann invariants determined the value for $\omega_2(0, t)$ as described below.

Denote as ω_{1_c} and ω_{2_c} the calculated values for $\omega_1(0, t)$ and $\omega_2(0, t)$ at each time step. The inflow Riemann invariant $s_1(0, t)$ must be specified, while the outflow Riemann invariant $s_2(0, t)$ cannot be specified, or the left boundary value will

be overimposed. In system (2.8), the value of $\omega_1(0, t)$ is known, but the value of $\omega_2(0, t)$ is not, so unfortunately the value of s_1 in Eq. (2.13) cannot be imposed. To compensate, we calculated the value of s_{2_c} in Eq. (2.13) by

$$s_{2_c} = \frac{\omega_{2_c}}{\omega_{1_c}} - 2\sqrt{\frac{\omega_{1_c}}{1 - L(t)}},$$

and then imposed $\omega_1(0, t) = 1 - L(t)$ to arrive at

$$s_{2_c} = \frac{\omega_2(0, t)}{\omega_1(0, t)} - 2\sqrt{\frac{\omega_1(0, t)}{1 - L(t)}},$$

which can then be solved for $\omega_2(0, t)$.

The evaluation of the boundary points and the approximation of $L'(t)$ and $L(t)$ are more natural for the Chebyshev collocation method than for finite difference methods, since they are implicitly evaluated in the method, rather than extrapolated from other interior points.

4. VERIFICATION OF NUMERICAL METHODS: A TEST CASE

The suitability of the numerical schemes described in Section 3 to system (2.8) and therefore system (2.1) was verified by studying a similar example for which the analytical solution is available and the numerical calculations can be verified.

By slightly modifying the initial and boundary conditions of system (2.8), the problem is reduced to a system of differential equations to which an analytical solution can be found. The new initial and boundary conditions have no physical meaning but provides a good ''test'' case in order to verify the applicability of our numerical algorithms to the real problem. Recall the transformed system

$$\begin{aligned} \omega_{1_t} + \frac{1}{(1 - L(t))}((L'(t)\xi - t)\omega_1 + \omega_2)_\xi &= 0 \\ \omega_{2_t} + \frac{1}{(1 - L(t))}\left((L'(t)\xi - t)\omega_2 + \frac{\omega_2^2}{\omega_1} + \frac{\omega_2^2}{2(1 - L(t))}\right)_\xi &= 0, \end{aligned} \tag{4.1}$$

where $L'(t) = t - \omega_{2_\xi}/\omega_{1_\xi}$. Now suppose we are given the initial conditions

$$\begin{aligned} \omega_1 &= (1 - L(0))(1 - \xi) \\ \omega_2 &= 0 \end{aligned}$$

and the boundary conditions

$$\omega_1(0, t) = \frac{(1 - L(t))^2}{1 - L(0)}$$

TABLE I
L_2 Norm Errors for ω_1 and ω_2 Using the MacCormack Method for $N = 20$, 40, and 80 Points and Total Time $t = 1.0$

N	$L_2\omega_1$	$L_2\omega_2$	Time steps	CPU time
20	8.9E-4	1.1E-3	25	0.02
40	3.3E-4	4.0E-4	50	0.04
80	1.4E-4	1.6E-4	100	0.10
3200	2.6E-6	2.9E-6	4001	115.7

$$\omega_2(0, t) = \left(\frac{1 - L(t)}{1 - L(0)}\right)^2 t$$

$$\omega_1(1, t) = 0$$

$$\omega_2(1, t) = 0.$$

An exact solution to system (4.1) system to the above conditions is

$$\omega_1(\xi, t) = \frac{(1 - L(t))^2}{1 - L(0)}(1 - \xi)$$

$$\omega_2(\xi, t) = \frac{(1 - L(t))^2}{1 - L(0)} t(1 - \xi)$$

$$L(t) = L(0)\left(1 - \frac{t^2}{2(1 - L(0))}\right).$$

System (4.1) was numerically solved using both the MacCormack finite difference scheme and the spectral Chebyshev collocation method. For consistency purposes, the numerical experiments were performed assuming no knowledge of $\omega_2(0, t)$, since $v_2(0, t)$ is unknown in system (2.8).

The numerical spatial order of accuracy is displayed in Table I while Table II shows the numerical temporal order of accuracy of the MacCormack scheme solving system (4.1). The first two columns are the L_2 norm errors of ω_1 and ω_2 and the third column is the absolute error for the variable $L(t)$. The drop to first-order

TABLE II
Temporal Accuracy for the MacCormack Method for $N = 20$ Points for Δt Fixed and Total Time $t = 1.0$

Δt	$L_2\omega_1$	$L_2\omega_2$	$L(t)$	Total time steps	CPU time
4.0E-2	8.9E-4	1.1E-3	4.9E-4	25	0.02
2.0E-2	3.2E-4	3.8E-4	1.5E-4	50	0.03
1.0E-2	1.3E-4	1.5E-4	5.0E-5	100	0.04

TABLE III

L_2 Norm Errors for ω_1 and ω_2 Using the Chebyshev Collocation Method for $N = 20$, 40, and 80 Points and Total Time $t = 1.0$

N	$L_2\omega_1$	$L_2\omega_2$	Time steps	CPU time
10	1.7E-07	2.2E-07	50	0.09
20	1.1E-08	1.4E-08	200	0.61
40	7.2E-10	9.0E-10	801	7.82
80	1.8E-10	2.3E-10	3200	114.8

accuracy in Table II is a result of not being able to calculate $L''(t)$ in the intermediate step of the MacCormack scheme.

Tables III and IV display the numerical spatial and temporal order of accuracy for the Chebyshev method, which obtained spectral accuracy. The first two columns are the L_2 norm errors for ω_1 and ω_2 and the third column is the absolute error for the variable $L(t)$.

The CPU times for solving system (2.8) are practically the same for $N = 3200$ for the MacCormack method and $N = 80$ for the Chebyshev method. This is easily understood since the CPU time is proportional to the number of time steps and for the MacCormack method $\Delta t \sim 1/N$ while for the Chebyshev method $\Delta t \sim 1/N^2$. The computational costs at each time step are marginal for both methods. In this example, the MacCormack method yields good results and is clearly less expensive. However, if greater accuracy is desired, then the Chebyshev method is the better choice, implying that it may also be more suitable for system (2.8).

5. THE NUMERICAL RESULTS

We solved system (2.8) for times up to $T = 100$ in nondimensional units using 80 grid points in the Chebyshev method and 3200 points in the MacCormack method. Comparable results were obtained for the MacCormack and the Chebyshev methods.

Most interesting is the evolution of $L(t)$, the time-dependent distance from the shoreline to the point where the total depth of the water vanishes, or equivalently,

TABLE IV

Temporal Accuracy for the Chebyshev Collocation Method for $N = 20$ Points and Total Time $t = 1.0$

Δt	$L_2\omega_1$	$L_2\omega_2$	$L(t)$	Time steps	CPU time
5.0-03	1.1E-08	1.4E-08	5.1E-09	200	0.61
2.5-03	6.7E-10	8.7E-10	3.0E-10	400	1.17
1.25-03	4.2E-11	5.4E-11	1.9E-11	800	2.28

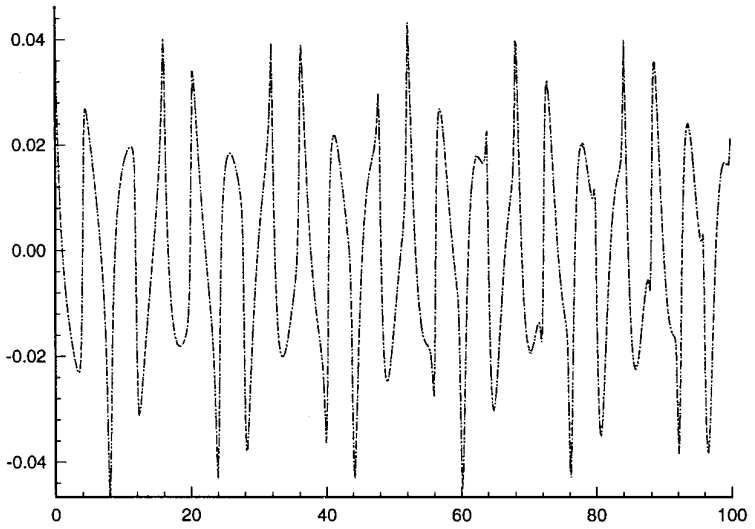

FIG. 3. Time Series for $L(t)$ using MacCormack and the Chebyshev methods. It is nearly impossible to detect a difference in the results.

the receding distance of dry land. The MacCormack and the Chebyshev schemes yield almost identical results, as shown in Fig. 3.

Since the graph of the time series of $L(t)$ in Fig. 3 exhibits oscillatory behavior, we analyzed the data set of $L(t)$ for its frequency spectrum using a discrete fast Fourier transform technique [1]. First, the time-averaged value $L(t)$ was subtracted from the data to form a time sequence p_j of N points for $N = 2^m$ for some positive integer m (here $m \sim O(9)$). Then the Fourier coefficients f_k of the transformation

$$f_k = \sum_{j=0}^{N-1} p_j e^{\frac{-i2\pi jk}{N}}$$

for $k = 0, \ldots, N-1$ were computed. The power spectral density d_k for wavenumber k is then simply

$$d_k = |f_k|^2,$$

corresponding to the nondimensionalized frequency, $k/N\Delta t$, where $\Delta t = T/N$ and T is the total time.

Figure 4 displays the spectral power density for the Chebyshev and the MacCormack methods. The largest signal is at 0.2, followed by smaller peaks at 0.45 and 0.7.

In Fig. 5 the spectral density of $L(t)$ is compared to the situation where the wall is placed at $x_0 = 0.95$ and $L(t) = -\eta(x_0, t)$ measures the depression of the water at the wall. It is evident that the first and largest signal has nearly the same amplitude but is slightly shifted in the "wall" case. The effect of the wall on subsequent peaks is much more drastic. We can therefore conclude that the first peak at the lower frequency is associated with the basin's geometry while the beating frequency which

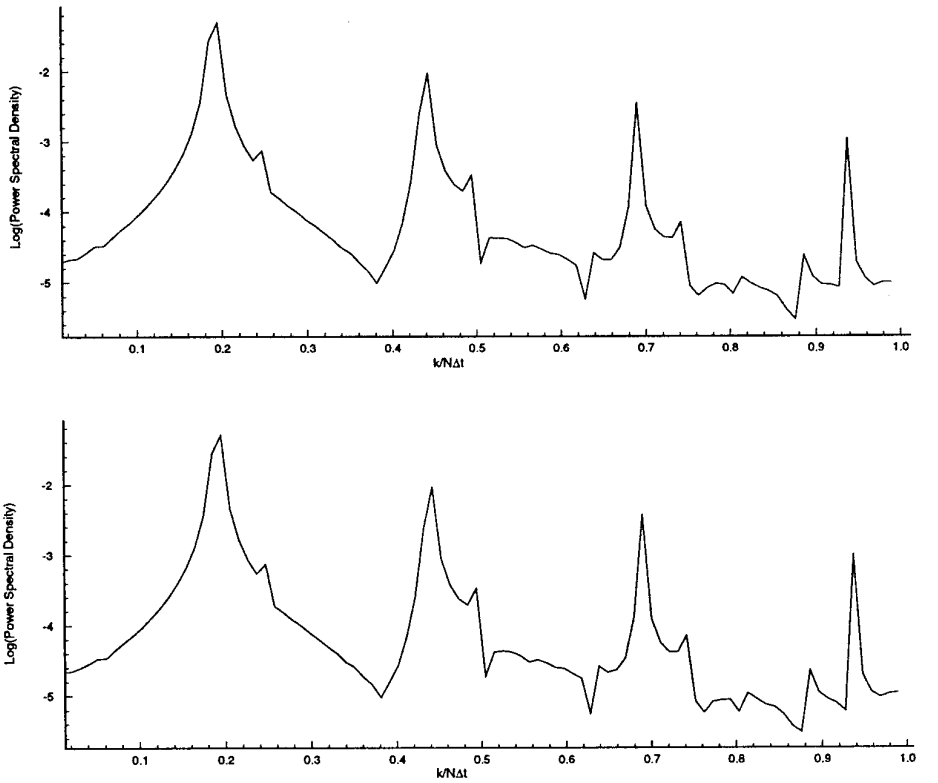

FIG. 4. Spectral density graph of $L(t)$ using (a) Chebyshev and (b) MacCormack methods.

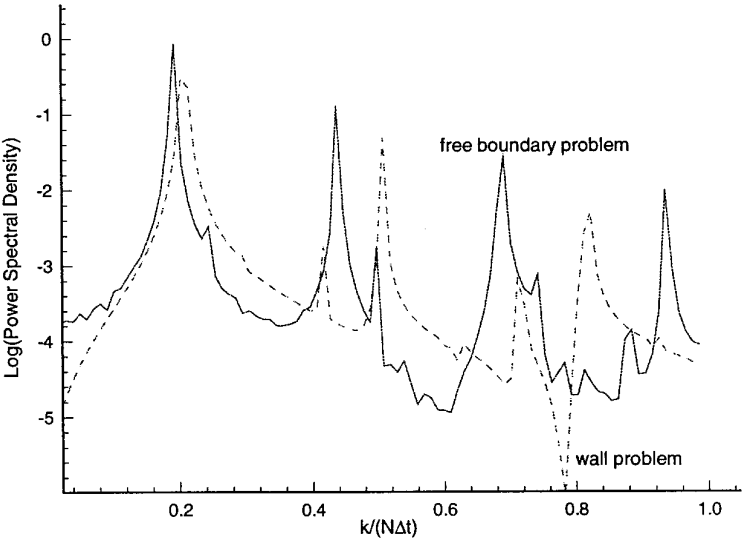

FIG. 5. Spectral density graph of $L(t)$ for no wall and for when a wall is placed at $x_0 = 0.95$.

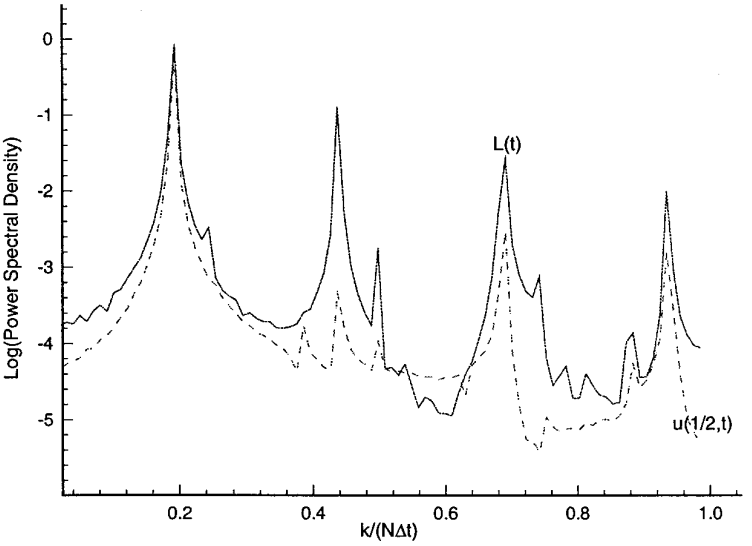

FIG. 6. Spectral density graph of $L(t)$ and $u(\frac{1}{2}, t)$.

determines the distance (i.e., frequency difference) to the secondary peaks is related to the dynamics of the singular point at the boundary. The other effect of the singular boundary is the slight increase in the height of all spectral peaks including the first.

It is evident that u and η also exhibit oscillatory behavior at each spatial point. The spectral peak at 0.2, which is so dominant in the time series of $L(t)$, is clearly dominant in both the velocity and the sea surface spectrum at the midpoint $x = 1/2$ as shown in Figs. 6 and 7. While the second peak of the spectrum of $L(t)$

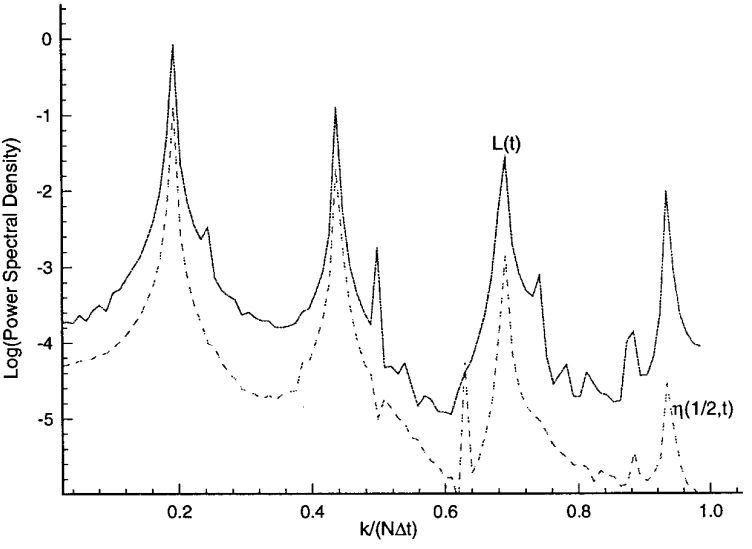

FIG. 7. Spectral density graph of $L(t)$ and $\eta(\frac{1}{2}, t)$.

characterizes the spectrum of $\eta(1/2, t)$, it is absent from the spectrum of $u(1/2, t)$. The fact that the behavior of $\eta(1/2, t)$ follows $L(t)$ more closely than that of $u(1/2, t)$ is understandable since $L(t) = -\eta(1 - L(t), t)$.

The Chebyshev and the MacCormack methods also yielded similar results for the spatial values of $u(x, t)$ and $\eta(x, t)$; however, there were small discrepancies at the right boundary. The spatial results of $u(x, 10)$, $\eta(x, 10)$, $u(x, 40)$, and $\eta(x, 40)$ are seen in Figs. 8 and 9. The structures vary considerably with time and very sharp gradients persist near the right singular boundary.

We feel that the Chebyshev method provides better solution for several reasons. First, the Chebyshev method is less likely to suffer from roundoff error since fewer points are required to obtain a solution than in the MacCormack method. Second, the Chebyshev method solved $L'(t)$ inherently, while a less natural extrapolation at the boundary was required for the MacCormack method. Third, the L_2 error analysis for system (4.1) indicates that the numerical performance of the Chebyshev spectral scheme is better suited to this type of problem. However, the similarity of the results using both the MacCormack scheme and the Chebyshev collocation method indicates the validity of the solution for either method.

6. DISCUSSION

The results presented in the Section 5 point to the important finding that no shocks form as the wind ceases to apply the stress at the surface of the gulf, allowing the water to flow freely subject only to the pressure gradient force. In this sense, the problem is similar to the classical dam break problem where a dam is released and the water is allowed to flow freely down the pressure gradient. As no general criterion is available to *a priori* determine whether such shocks will or will not develop, our findings rule out the possibility that the nonlinear terms in the model equations will general shocks.

The water will oscillate up and down the beach rather than develop discontinuities, and since no viscosity was introduced in our model, these oscillations can persist for a very long time. The frequency of these up-and-down oscillations equals the speed of gravity waves propagating into the gulf from the open ocean divided by twice its length. This speed is given, at any point x, and time t, by $[1 - x + \eta(x)]^{1/2}$ (and in dimensional form $[g(D/l \times (l - x) + \eta(x))]^{1/2}$). Since the length of our gulf is 1.0 for $\eta = 0 = u$, the value of 0.2 shown in Fig. 4 as the first peak in the spectrum represents a weighted average of the speeds at the various points along the gulf. This averaged frequency could not be determined from any other considerations since it is not clear whether it is the speed or the water depth which has to be averaged. The only way to calculate the speed in cases where the geometry is not simple enough (e.g., uniform) is to perform direct numerical calculations such as those presented in this work. This mode of water ocillations owes its existence to the *geometry* of the gulf and not to the particular initial conditions we used, as is evident from the comparison shown in Fig. 5, where the same peak at a frequency of 0.2 prevails for the "wall" case as well as for the relaxation of the

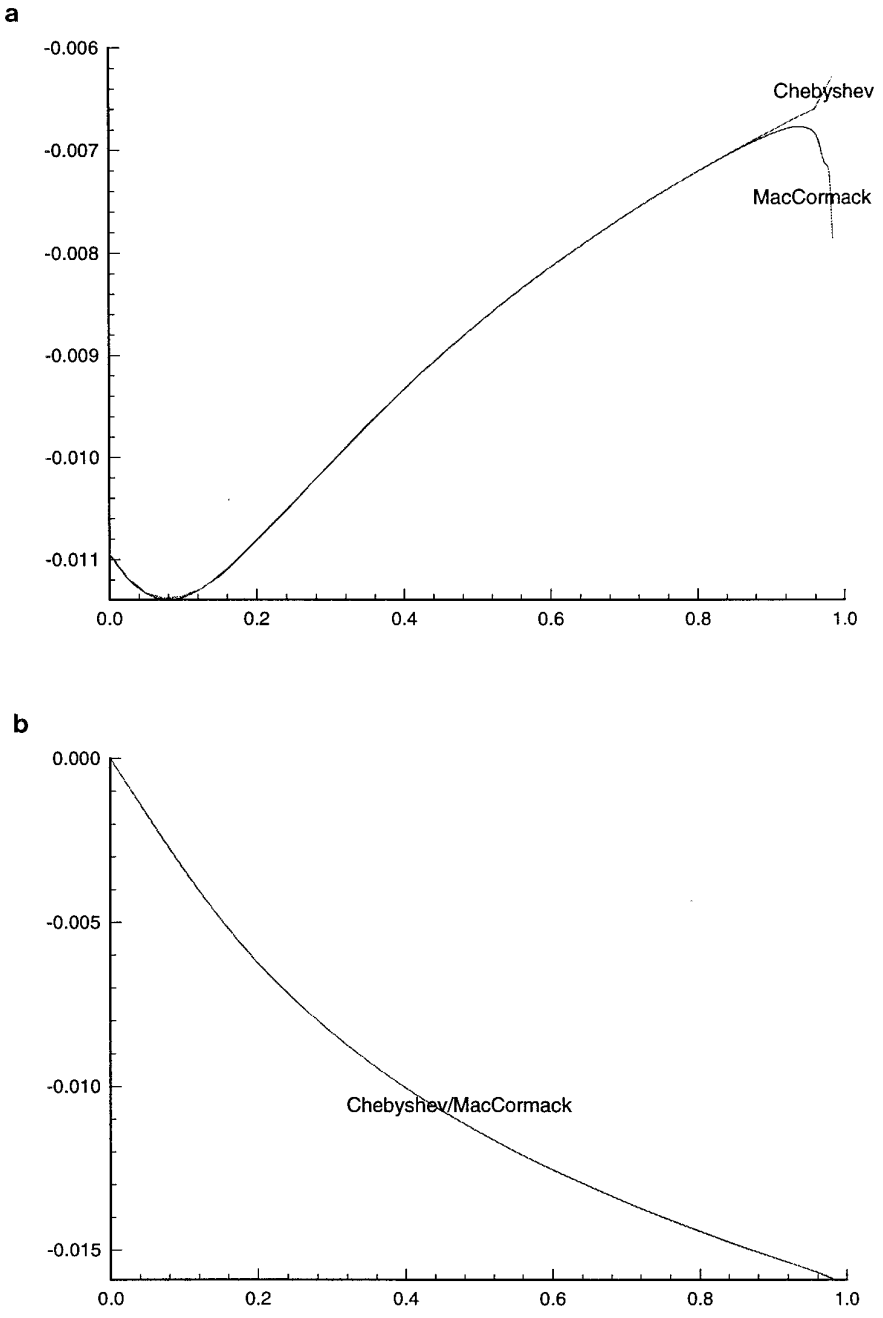

FIG. 8. Solution at (a) $u(x, 10)$ and (b) $\eta(x, 10)$.

wind set-down case. The effect of the singularity associated with the latter manifests itself in the beating frequency which determines the frequency difference between the aforementioned main peak and its subharmonics which appear very clearly in the spectrum.

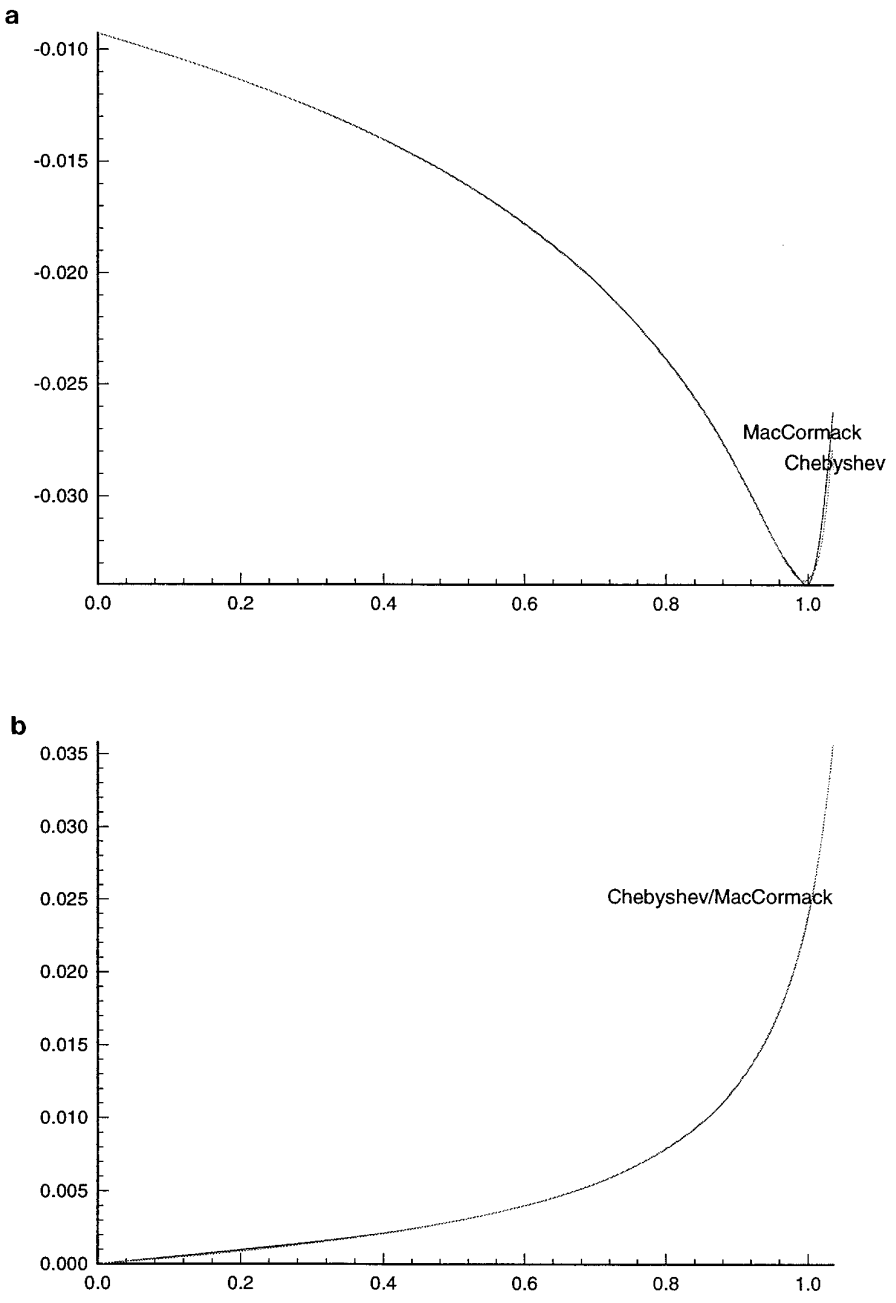

FIG. 9. Solution at (*a*) $u(x, 40)$ and (b) $\eta(x, 40)$.

An interesting result which emerges from our calculations is that the water can climb up and down the beach to distances which exceed the original distance, $L(0)$. The required water mass as well as potential energy are supplied, of course, by the infinite ocean at $x < 0$.

Our work lends credence to the approach in [8], where the problem of tsunami propagation was solved on a sloping beach by ignoring the dynamics associated with the singularity of the nose. As demonstrated in this study, neglecting the singularity only affects the secondary peaks in the spectrum but has no effect on the main peak there.

The application of our results to the Gulf of Suez, which have the same wind stress and geometric parameters for the study of the steady-state solution described in [10], implies that the water will run up the shore a dimensional distance of 14 km for an $l = 350$ km gulf (see Fig. 3). This will take place in about 30 h for $D =$ 70 km after the wind stopped blowing. The typical water speed associated with this behavior is about 2.5 m/s which is approximately 5 knots. These velocity values are reasonable given the highly idealized assumptions made here, specifically that the strong winds turn to a complete calm instantaneously, the slope of the bottom of Gulf is perfectly linear for 350 km and no drag is being exerted by the bottom on the overlying water.

Both numerical schemes employed here, the MacCormack finite difference scheme and the spectral Chebyshev method, yield accurate results for our problem in spite of the loss of strong hyperbolicity at the point of diminishing water. There is some discrepancy of these solutions due to the numerical solution at the boundary. The Chebyshev method probably yields more accurate results since it is a global method and the approximation of the boundary values is built implicitly into the scheme. On the other hand, the MacCormack scheme, which is local, extrapolates information from neighboring points to approximate the solution at the boundary. The inaccuracy of this approximation contaminates the neighboring points, which in turn affects the accuracy at the boundary. Eventually this can affect the results over the entire domain. Therefore many points are required for the MacCormack scheme to ensure accuracy at the boundary. Far fewer points are required for the Chebyshev method, making it less susceptible to computational roundoff error.

ACKNOWLEDGMENTS

The authors express their appreciation to Eitan Tadmor for his insight and ideas, which were essential for the completion of this project. The authors were supported by AFOSR Grant F49620-95-1-0074, NSF Grant DMS 9500814, and DARPA/ONR AASERT Grant N00014-93-1-0985. Nathan Paldor also acknowledges the Israel Academy of Sciences for making this research possible by providing a grant to the Hebrew University.

REFERENCES

1. S. Abarbanel, W. S. Don, D. Gottlieb, D. H. Rudy, and J. C. Townsend, Secondary frequencies in the wake of a circular cylinder with vortex shedding, *J. Fluid Mech.* **225** (1991).
2. L. Egnesund, ''The Shallow-Water Equations in a Water-Course with Sloping Shores Extended with an Artificial Water Domain,'' Uppsala University, Department of Scientific Computing, Report No. 124, 1989.
3. G. F. Carrier and H. P. Greenspan, Water waves of finite amplitude on a sloping beach, *J. Fluid Mech.* **4,** 97 (1958).

4. P. Glaister, An approximate linearized Riemann solver for the Euler equations for real gases, *J. Comput. Phys.* **74** (1988).
5. D. Gottlieb, M. Y. Hussaini, and S. Orszag, Theory and applications of spectral methods, in *Spectral Methods for Partial Differential Equations*, edited by R. C. Voigt, D. Gottlieb, and M. Y. Hussaini (SIAM, Philadelphia, 1984), p. 1.
6. D. Gottlieb and S. Orszag, *Numerical Analysis of Spectral Methods: Theory and Applications,* NSF-CBMS Monograph No. 26 (SIAM, Philadelphia, 1977).
7. H. P. Greenspan, On the breaking of water waves of finite amplitude on a sloping beach, *J. Fluid Mech.* **4** (1958).
8. S. Hibberd, and D. H. Peregrine, Surf and run-up, in *Waves on Water of Variable Depth*, edited by Provis and Radok, Lecture Notes in Physics (Springer-Verlag, Berlin/New York, 1976).
9. K. Kajiura, Local behavior of tsunamis, in *Waves on Water of Variable Depth*, edited by Provis and Radok, Lecture Notes in Physics (Springer-Verlag, Berlin/New York, 1976).
10. D. Nof and N. Paldor, Are there oceanographic explanations for the Israelites' crossing of the Red Sea? *Bull. Amer. Meteorological Soc.* **73,** 3 (1992).
11. J. J. Stoker, Formation of breakers and bores, *Comm. Pure Appl. Math.* **1,** 1 (1948).
12. E. O. Tuck and L.-S. Hwang, Long wave generation on a sloping beach, *J. Fluid Mech.* **51,** 3 (1972).